Journal of the European Ceramic Society 38 (2018) 2579–2587

Contents lists available at ScienceDirect

Journal of the European Ceramic Society

journal homepage: www.elsevier.com/locate/jeurceramsoc

Original article

Substrate-constrained effect on the stiffening behavior of lamellar thermal barrier coatings

Guang-Rong Li, Juan Lei, Guan-Jun Yang*, Cheng-Xin Li, Chang-Jiu Li

State Key Laboratory for Mechanical Behavior of Materials, School of Materials Science and Engineering, Xi'an Jiaotong University, Xi'an, Shaanxi Province 710049, PR China

ARTICLE INFO

Keywords:
Substrate constraint
Constrained healing
Stiffening
Thermal barrier coatings
Structural evolution

ABSTRACT

Thermal exposure would compromises the compliance and thermal insulating performance of thermal barrier coatings (TBCs). However, most publications were based on free-standing coatings in which the stress resulting from substrate is essentially different from TBCs on superalloy substrate. In this paper, the constrained effect of substrate on the ceramic top-coat of plasma sprayed lamellar TBCs was investigated. Results showed that the structural changes evolve from micro-scale to macro-scale during thermal exposure. In a relatively shorter thermal exposure stage, the inter-splat pores became narrowed, whereas the intra-splat cracks became widened. Consequently, the healing kinetics of inter-splat pores was much faster than that of the intra-splat cracks. In a relatively longer thermal exposure stage, some macroscale cracks appeared in coating surface owing to the gradually stiffening coatings. As a result, the microscale intra-splat cracks near the macroscale cracks were healed rapidly. In brief, the substrate constraint induced structural changes were stage sensitive.

1. Introduction

Plasma-sprayed ceramic coatings, such as yttria stabilized zirconia (YSZ), has been widely used as the top coat of thermal barrier coatings (TBCs) on hot section parts for aircraft engine and land-based gas turbine, owing to its excellent performance of thermal insulation and strain tolerance [1–5]. The thermal exposure often leads to some degradation on performance with increasing risk of spallation due to sintering and associated stiffening of the YSZ top coat, which is strongly indicated by many papers on evolution of microstructure and mechanical property of YSZ coatings [6–12]. Most studies were focused on free-standing YSZ coatings detached from substrate, since the free-standing sample is convenient for experiments, especially for the measurement of thermal properties and mechanical properties. However, this simplification ignores some important factors, such as the stresses generated from substrate.

The stresses can be analyzed after the coating deposition and during the post thermal exposure. After the coating deposition, some residual stress can be generated in plasma sprayed YSZ coatings resulting from two major sources [13,14]. The first is quenching stress resulting from the cooling contraction of splat. Intra-splat cracks relax some quenching stress, reducing the stress from theoretical several GPa to tens of MPa. The second is thermal stress resulting from the mismatch of thermal expansion coefficient (CTE) between YSZ coatings and substrate during post-deposition cooling from a possible elevated temperature to room temperature. This thermal stress is usually compressive stress due to the lower CTE of YSZ (about $11.5{\cdot}10^{-6}\,K^{-1}$) than that of Ni-based superalloy (about $15{\cdot}10^{-6}\,K^{-1}$) [10,15]. The final residual stress is usually tensile stress at room temperature [16,17]. During post thermal exposure, some extra CTE mismatch stress would be generated in YSZ coatings. Therefore, the residual tensile stress may be enhanced during further thermal exposure.

Several previous studies focusing on constrained sintering of ceramic coatings have shown some global trends with experiments and models. Tillman et al. [18] reported the stress development during isothermal treatment with alumina film constrained by alumina substrate. Their results showed that the sintering in out-plane direction was enhanced compared with that in in-plane direction. Wang et al. [19] characterized the microstructural evolution of zirconia films attached to zirconia substrate, showing partial densification after cracking. A series of papers gave insight into the densification rate to reveal kinetics of constrained sintering compared with free sintering, which present a strong effect of the substrate constraint on sintering [15,20,21]. These studies have revealed some general trends on constrained sintering with nearly isotropic structure. However, plasma sprayed YSZ coatings exhibit anisotropic lamellar structure including inter-splat pores and intra-splat cracks [22–24]. That's why the thermal- and mechanical-properties in in-plane direction are distinct larger than those in out-

* Corresponding author.
E-mail address: ygj@mail.xjtu.edu.cn (G.-J. Yang).

https://doi.org/10.1016/j.jeurceramsoc.2018.01.028
Received 28 July 2017; Received in revised form 11 January 2018; Accepted 16 January 2018
Available online 31 January 2018
0955-2219/

plane direction [25,26]. Therefore, the global densification rate or shrinkage cannot stand for the real response of plasma-sprayed YSZ coatings exposed to high temperature. It is highly necessary to have a deep understanding on the structural evolution of plasma sprayed YSZ coatings based on their unique microstructure.

The unique lamellar coatings with multiscale, multi-morphology pores brings half more drop of in-plane Young's modulus [6,8,26,27] and out-plane thermal conductivity [28] with respect to those of the bulk YSZ material. Moreover, the stiffness of the coatings is highly dependent on the applied strain [29]. All these features are substantially contributed by the 2-dimensional (2D) shaped inter-splat pores and intra-splat cracks [29–32]. The inter-splat pores generally correspond to the imperfect bonding between splats. That's why the plasma sprayed ceramic coatings exhibit approximately 30% bonding ratio without a preheating treatment on substrate [24,33]. In contrast, the intra-splat cracks are generated during splat quenching to relieve thermal stress. Consequently, the disk-shaped splats are divided into amount of segments [10,34]. Moreover, the inter-splat pores are connected with the intra-splat cracks [23].

In the case of constrained sintering for plasma sprayed YSZ coatings, Cipitria et al. [35] developed a sintering model to show the sintering progress constrained by rigid substrate. Cocks et al. [36] also proposed a model to investigate the constrained sintering of plasma sprayed YSZ coatings. Coin-shaped cracks with variational directions were proposed in their model. These two studies make significant contribution to understanding the constrained sintering of plasma sprayed YSZ coatings from the perspective of 2D cracks existing in lamellar structure. Nevertheless, a sufficient microscopic view on healing of inter-splat pores and intra-splat cracks constrained by substrate has not been presented yet. The cracking mechanism due to the stress during thermal exposure is still unclear for plasma sprayed YSZ coatings.

The objective of this study is to reveal the response of YSZ coatings attached to substrate during thermal exposure. In particular, this study focus on the healing of microscale 2D pores and cracks, with the aim to comprehensively understand the constrained sintering of plasma sprayed YSZ coating.

2. Experimental

2.1. Experimental materials

A commercially available hollow spherical 8 wt% YSZ powder (HOSP, −75 to +45 μm, Metco 204B-NS, Sulzer Metco Inc., New York, USA, see Fig. 1a) was used to prepare the top-coat. Nickel-based superalloy (Inconel 738, Beijing Cisri-Gaona Materials & Technology Co., Ltd., Beijing, China) was used as substrates. Before the top-coat deposition, NiCoCrAlTaY (~37 μm, Amdry 997, Sulzer Metco, New York, USA) was used to prepare the bond-coat preferentially on substrate.

It is easier for the fused-crushed powder to get complete individual splat with little splashing compared with HOSP powders. Therefore, another fuse-crushed YSZ powder (FC, 5–25 μm, AMPERIT 825, H.C. Starck, Germany, see Fig. 1b) was used to deposit individual splats. Morphologies of these two powders are shown in Fig. 1. Individual YSZ splats were formed on bulk magnesia substrate, in order to investigate the fundamental microstructural changes of the plasma sprayed YSZ coatings. The CTEs of Ni-based superalloy, magnesia, and YSZ are approximately $15{\cdot}10^{-6}\,K^{-1}$, $14{\cdot}10^{-6}\,K^{-1}$ and $11{\cdot}10^{-6}\,K^{-1}$, respectively.

2.2. Sample preparation

Bond coat with a thickness of ~100 μm was deposited by low pressure plasma spraying (LPPS) at a powder feeding rate of 19 g/min. After the deposition of bond-coat, a pre-annealing treatment of the samples was carried out at a temperature of 1000 °C for 4 h followed by a further annealing at 1080 °C for 4 h in an argon atmosphere. Consequently, a uniform layer of α-alumina-based thermally growth oxide (TGO) was formed in top surface.

The top coat was deposited by air plasma spraying (APS) using a commercial plasma spray system (GP-80, 80 kW class, Jiujiang, China) to a thickness of 500 μm to conduct the properties test and structure observation. As a comparison, free-standing YSZ coatings were obtained using stainless steel as substrate through post-spray dissolving the substrate by a hydrochloric acid solution. Spray parameters of the APS and the LPPS are shown in Table 1.

2.3. Thermal exposure of samples

In order to highlight the possible microstructural changes induced by the effect of substrate constraint, isothermal test was used in this study. It should be noted that, in real service condition, the temperature of substrate would be lower than that of the top-coat, since the substrate is cooled. Given that, the effect of CTE mismatch would be overestimated slightly using isothermal test. However, the isothermal test facilitates the observation on microstructural changes.

Commonly, the working temperature for TBCs is approximately 1000–1100 °C. Therefore, the samples were isothermally heat treated to a temperature of 1100 °C. After progressively holding for different durations, the samples were cooled down to room temperature. Based on previous reports [37,38], the significant formation of monoclinic phase often occurs at higher temperatures above 1200 °C. Therefore, it is reasonable to conclude that the sintering at 1100 °C is relatively unaffected by the phase change.

2.4. Microstructural characterization of YSZ deposits

Surface and cross-sectional morphologies of the YSZ coatings were examined using a scanning electron microscope (SEM) system (TESCAN MIRA 3, Czech). The healing behavior of 2D pores was characterized by a quasi in-situ observation with SEM. The details can be found elsewhere [39]. Cross-sectional samples of the individual splats were prepared using a focused ion beam system (Helios Nano Lab 600i dual-beam, America) [40]. In order to investigate the pore healing

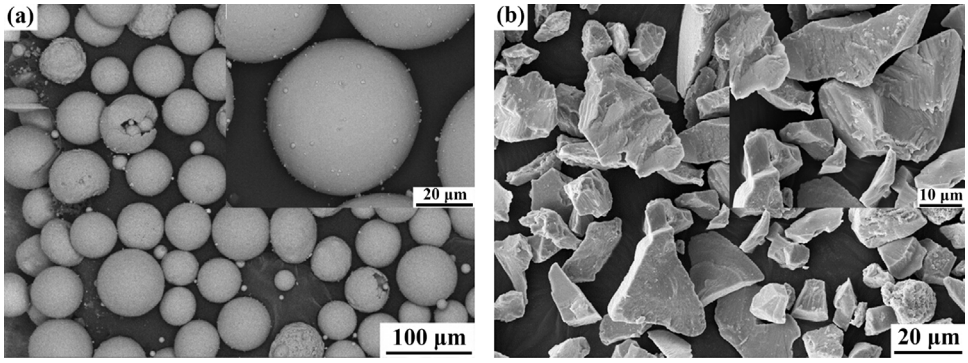

Fig. 1. Morphologies of the powders: (a) HOSP and (b) FC.

Table 1
Spray parameters of the APS and the LPPS.

Parameters	LPPS	APS
Plasma arc voltage/V	72	70
Plasma arc current/A	620	600
Flow rate of primary gas (Ar)/L·min^{-1}	40	50
Flow rate of secondary gas (H_2)/L·min^{-1}	8	7
Flow rate of powder feeding gas/L·min^{-1}	Ar/2	N_2/7
Chamber pressure/kPa	15	/
Spray distance/mm	160	110
Torch traverse speed/mm·s^{-1}	100	800

quantitatively, 2D pore density, defined as the total length of 2D pores in unit area, was determined in this study. The densities of inter-splat pores and intra-splat cracks were obtained from the polished cross-section and the polished surface of YSZ coatings, respectively. At least 100 SEM images at a magnification of ×5000 were determined.

2.5. Measurement of properties

Ionic conductivity of oxygen in YSZ was determined on Potentiostat (Solartron SI1287, Hampshire, England) by a direct current method. All samples to be tested were detached from substrate by immersion in 36% HCl. Before testing, platinum paste was plastered uniformly in an area of φ8 mm on both sides of the samples, ensuring that the centers of the two circles are coincident. Then the samples were heated in a furnace with a heating rate of 8 °C/min to 850 °C holding for 30 min to solidify platinum paste. The other details can be found elsewhere [41].

The hardness test was conducted on a microhardness tester (Buehler Micromet5104, Akashi Corporation, Japan) at a test load of 300 gf holding for 30 s.

The ionic conductivity of YSZ materials is sensitive to their grain boundary, chemistry, as well as microstructure. During thermal exposure, sintering may lead to grain growth, along with the reduction of grain boundaries. This would decrease the intergrain resistivity [42,43]. However, the thermal exposure related to ionic conductivity is only 2 h at 1100 °C. Therefore, the effect of grain growth would be much slight. Regarding the intragrain resistivity, there are no changes in compositions and crystalline structure during thermal exposure at 1100 °C [38,44]. Therefore, it is confirmed that the changes in the ionic conductivity of YSZ deposits after heat treatment would be attributed primarily to microstructural changes [41].

It is worth noting that the plasma sprayed ceramic coatings exhibit typical lamellar structure with intersplat pores, intrasplat cracks, as well as globular voids [34]. During thermal exposure, the porosity remains relatively unchanged, whereas the mechanical/thermal properties increase significantly [10,24,39]. That's why the change in porosity cannot be responsible essentially for the properties changes [24,45]. Therefore, the primary microstructural changes are related to the intersplat pores and intrasplat cracks, which would affect the ionic conductivity dominantly.

3. Results and discussion

3.1. Evolution of mechanical property after short thermal exposure

Fig. 2 shows the changes in hardness of YSZ coatings sprayed on substrates of YSZ and Ni-based superalloy after different thermal exposure durations at 1100 °C. The hardness of free-standing coatings was also determined for comparison. In the case of the free-standing coatings, the hardness increased with duration in both in-plane direction and out-plane direction. The increase rates slowed down from 10 h to 30 h with respect to that from as-deposited state to 10 h. This is consistent with previous reports [10,39], which revealed that the sintering kinetic at initial stage (approximately 10 h) is much higher than that in the following stage. The hardness evolution of coatings attached to substrates (YSZ and Ni-based alloy) exhibit similar trends compared with free-standing coatings. However, the increase rates are different. In the case of the hardness in out-plane direction of the YSZ coatings attached to Ni-based superalloy, the increasing rate was higher than that of the free-standing coatings. In the case of the hardness in in-plane direction of the YSZ coatings attached to Ni-based superalloy, the increasing rate was much lower than that of the free-standing coatings. In the case of the coatings attached to YSZ substrate, the increase rates were located between free-standing coatings and coatings attached to Ni-based superalloy, since there was no CTE mismatch stress between YSZ coatings and YSZ substrate. To sum up, during thermal exposure, the substrate constraint leads to anisotropic evolution in hardness, i.e., an enhanced increase in out-plane direction, whereas a weakened increase in in-plane direction. Moreover, an extra tensile force (e.g., a CTE mismatch stress) intensifies this anisotropic evolution. It is reported that the mechanical property (e.g., stiffness) of plasma-sprayed YSZ would be affected by the opening and closure of micro-cracks and pores [29]. Therefore, healing of the 2D pores would be investigated.

3.2. Healing evolution of 2D pores after short thermal exposure

From the changes in mechanical properties during thermal exposure, anisotropic evolution trend can be found, which means the sintering kinetics at different directions may be different. Due to the fact that the sintering behavior of APS YSZ coatings is highly structure specific, herein the microstructural evolution will be firstly presented. Plasma sprayed YSZ coatings exhibit lamellar structure with connected inter- and intra-splat crack network. This is the intrinsic characteristic of plasma sprayed ceramic coatings [10,23,45]. The multi-scale and multi-orientation cracks (or pores) lead to the anisotropic properties of plasma sprayed ceramic coatings [10,45]. Based on the consideration above, the healing of inter-splat pores and intra-splat cracks would be examined.

Fig. 3 shows the healing behavior of intra-splat cracks on coating surface. From the initial morphologies observed in untreated states, it can be found that the widths of cracks were nearly in same scale and that the surfaces of splats are smooth. However, in the case of free-standing YSZ coating (see Fig. 3a), after thermal exposure, the narrower cracks have been healed up, while the two sides of the wider crack had an obvious trend to move together through severe roughening by grain growth. In the case of the YSZ coating attached to YSZ substrate, the width of crack remained even with slight roughening on two sides of cracks. Furthermore, the healing of the narrower cracks was also retarded observed from Fig. 3(b-3). In the case of the YSZ coating attached to Ni-based superalloy, instead of healing up or remaining the origin state, the crack became widened as a function of the thermal exposure duration.

In brief, in free-standing coatings, the intra-splat cracks are healed up gradually. However, when the coatings are attached to substrate, the healing of intra-splat cracks would be retarded. Moreover, the CTE mismatch stress enhances this trend. As mentioned in introduction, 2D cracks play a critical role on the mechanical and thermal properties [23,45]. Moreover, the morphology changes of cracks would affect the mechanical property significantly [29]. Therefore, most intra-splat cracks oriented vertically in coatings, which would have a significant effect on the hardness in out-plane direction [46]. The effect of substrate on the healing behavior of intra-splat cracks is consistent with the hardness evolution in in-plane direction (see Fig. 2b).

Fig. 4 shows the healing of inter-splat pores in fractured cross-section of YSZ coatings at 1100 °C for different durations. As the annealing duration increases, the smooth surface of inter-splat pores in the as-deposited state became roughening in all conditions due to the growth of columnar grains inside splats. This leads to the multi-point healing of the counter-surfaces of inter-splat pores [39]. However, in the case of the coatings attached to substrate, the width of inter-splat pores became

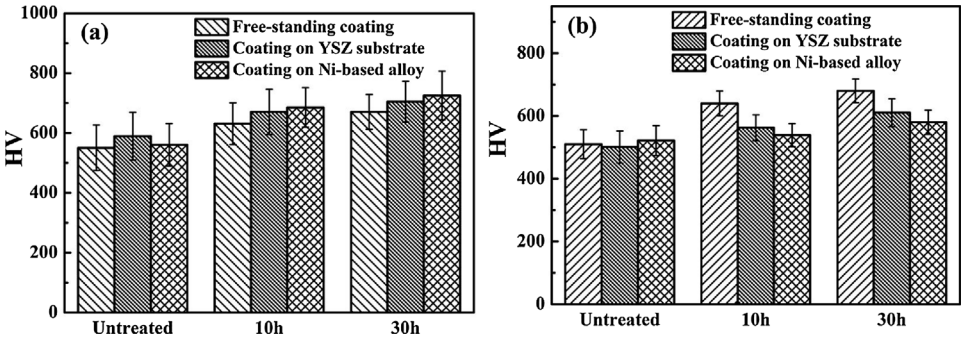

Fig. 2. Changes in hardness after thermal exposure: (a) in out-plane direction and (b) in in-plane direction.

narrowed, and thus it would be easier to connect by the grain growth. Therefore, the healing of inter-splat pores in the coating attached to substrate was enhanced with respect to that in the free-standing coatings. In the case of the YSZ coatings attached to Ni-based superalloy, the CTE mismatch between YSZ coatings and substrate results in extra strain when annealing at high temperature. Due to the lamellar structure and limited bonding ratio in plasma spray ceramic coatings [24,33], the bonding area between splats is the main carrier to transmit load from the interface between coating and substrate to the surface of coatings. The extra strain leads to further narrowing down of the inter-splat pores, and thus the healing of pores are further enhanced by the multi-point healing mechanism [39], as shown in Fig. 4(c-3). In brief, the effect of substrate leads to a faster healing kinetics of inter-splat pores owing to the constraint-induced narrowing of inter-splat pores. This can account for the hardness evolution in out-plane direction (see Fig. 2a).

Fig. 5 shows the statistical data on 2D pore healing as a function of thermal duration. It can be found that the densities of both inter-splat pores and intra-splat cracks decreased significantly in free-standing coatings. The substrate-constrained effect leads to much severer healing of the inter-splat pores, as shown in Fig. 5a. In contrast, the intra-splat cracks seemed unaffected when the coating is attached to substrate. Moreover, when there was a CTE mismatch between coating and substrate, the density of intra-splat cracks could even increase slightly, as shown in Fig. 5b. The changes on 2D pore densities were consistent with the direct observation on pore healing shown in Fig. 3 and Fig. 4.

3.3. Mechanism of morphology change of 2D pores during thermal exposure

The ionic conductivity of YSZ was related to its composition and microstructure [41]. The lower conductivity of plasma sprayed YSZ coatings with respect to that of bulk material is mainly attributed to its lamellar structure with limited bonding areas [47]. During thermal exposure, sintering may affect the ionic conductivity of coatings from two aspects. On one hand, sintering leads to grain growth. The reduction of grain boundaries would increase the ionic conductivity inside splats [42,43]. On the other hand, sintering results in the healing of pores or cracks, which enhances the ionic conductivity between splats. Regarding the ionic conductivity in plasma-sprayed ceramic coatings [41], the effect of changes in microstructure would be much more effective than that in grain boundaries. Moreover, the substrate-constrained effect would mainly affect the structural changes in coatings. Therefore, the healing effect would be mainly discussed in this study. Fig. 6 shows the ionic conductivity in out-plane direction for YSZ coatings. From Fig. 6a after thermal exposure at 1100 °C for 10 min, it can be found that, compared with as-deposited coatings, the free-standing coating resulted in a little higher ionic conductivity, whereas the coating attached to Ni-based superalloy exhibit obvious lower values. After thermal exposure at 1100 °C for 2 h, as shown in Fig. 6b, the ionic conductivity of YSZ coating attached to Ni-based superalloy increased to be comparable to that of the as-sprayed state. According to Fig. 4 and 5, after thermal exposure, the coatings on superalloy substrate have a higher inter-lamellar bonding with respect to that of the free-standing coatings. Correspondingly, the ionic conductivity should be higher for the coatings on superalloy substrate. However, at the beginning of thermal exposure (e.g., 10 min), the CTE mismatch stress between coating and substrate may lead to some changes in microstructure prior to sintering. This would lead to decrease in ionic conductivity.

Fig. 7 shows the morphologies changes of 2D pores after thermal

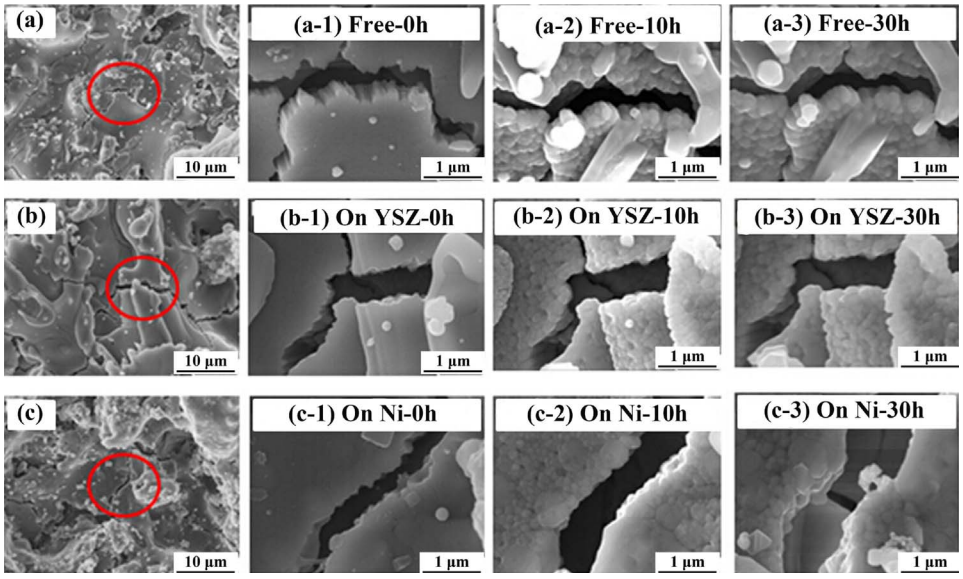

Fig. 3. Healing evolution of intra-splat cracks on coating surface during short thermal exposure: (a) free-standing coatings, (b) coatings attached to YSZ substrate, and (c) coatings attached to Ni-based superalloy.

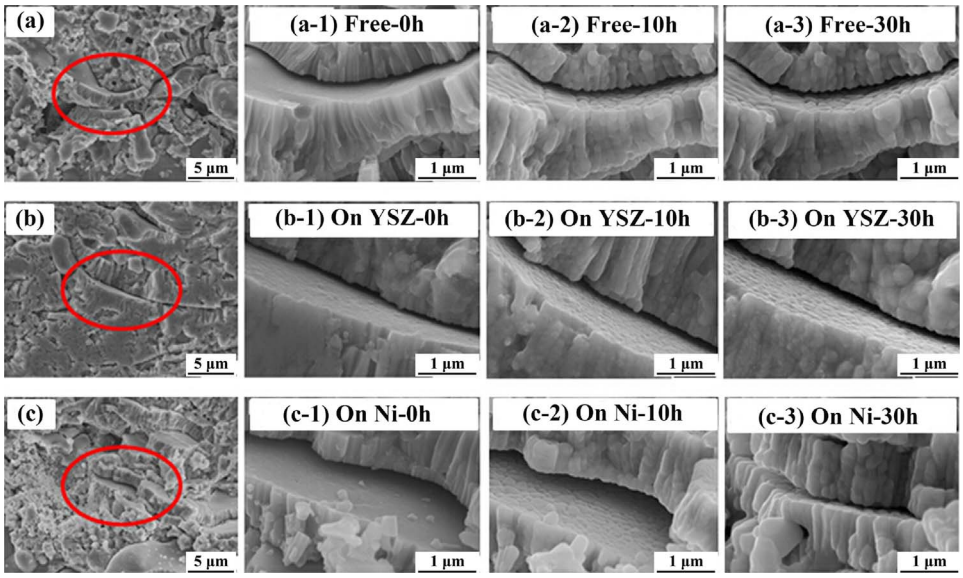

Fig. 4. Healing evolution of inter-splat pores on fractured cross-section during short thermal exposure: (a) free-standing coatings, (b) coatings attached to YSZ substrate, and (c) coatings attached to Ni-based superalloy.

exposure at 1100 °C for 10 min. The observation was conducted on individual splats deposited on magnesia substrate. In the case of the intra-splat cracks (see Fig. 7a), it can be observed that the intra-splat cracks became widened and that some cracks were extended. This can be responsible for the slight increase of intra-splat cracks shown in Fig. 5b. However, in the case of the inter-splat pores (see Fig. 7b), it can be found that the pore was extended along it tips.

Regarding the change mechanism of the 2D pores (or cracks), it is necessary to analyze the force transmission in YSZ coatings. Plasma sprayed ceramic coatings exhibit lamellar structure with limited bonding area between splats. Most cracks are connected with each other [45]. Therefore, the bonding areas are the main skeleton to support whole structure [24,33]. The schematics of plasma sprayed ceramic coatings attached to substrate with CTE mismatch stress is shown in Fig. 8a, and the region inside red circle is magnified as Fig. 8b, which stands for an inter-splat pore connected with an intra-splat crack. The forces in Fig. 8a mean the higher CTE of substrate than that of the coating. It can be found that the force applied on coating would be transmitted through the bonding areas, owing to the unique structure. According to our previous report [40], the force would transmit from the bottom layer to the top layer when applying an in-plane load on the substrate. During the force transmitting process, shear stress would be concentrated at the interface (bonding area) of two adjacent layers, whereas the force inside one layer would be primarily in tensile form, as shown in Fig. 9 [40]. This is consistent with other reports [48–50], which revealed that the interface between coating and substrate would bear shear stress dominantly. Based on the discussion above, the inter-splat pores would be extended further under the shear stress. This is consistent with other reports [51]. The widening of intra-splat cracks during initial thermal exposure was also related to the extension of the inter-splat pores. The extension of the inter-splat pores enlarges the non-bonded region, as shown in Fig. 8c, in which the red solid line stands for deformation from black dotted line. When cooling from annealing temperature, more area will shrink without restriction, which results in an unrecoverable widening of the intra-splat cracks.

Based on the discussion above, the CTE mismatch stress would result in further microstructural changes at the beginning of sintering, i.e., the extension in inter-splat pores and intra-splat cracks (see Fig. 7a). As a result, the starting microstructure of the coatings prior to sintering on Ni-based superalloy is actually different from that of the free-standing coatings. This is consistent with previous report [51]. The changes in ionic conductivity are highly dependent on the changes in microstructure. Therefore, the ionic conductivity decreased after a very short thermal exposure (see Fig. 6a). Subsequently, despite the fact that the healing of inter-splat pores is enhanced during thermal duration owing to the substrate-constrained effect (see Figs. 4 and 5a), it should take some time for the ionic conductivity in constrained coatings to exceed that in free-standing coating. This can be responsible for the phenomenon (see Fig. 6b) that the ionic conductivity in constrained coatings was lower than that in free-standing coatings in a short thermal duration (e.g., within 2 h).

To sum up, Fig. 10 shows the change mechanism of the 2D pores in plasma sprayed YSZ coatings attached to substrate. The main load from substrate was the CTE mismatch stress, which were transmitted through the bonding areas in shear form. As a result, the tips of inter-splat pores are further extended, as shown in c and c^1 in Fig. 10. The resulted more non-bonded area enhances the shrinkage without constraint and leads to unrecoverable widening of intra-splat cracks. The CTE mismatch stress also makes the inter-splat pores become narrowed, as shown in b and b^1 in Fig. 10. The narrowed inter-splat pores results in more

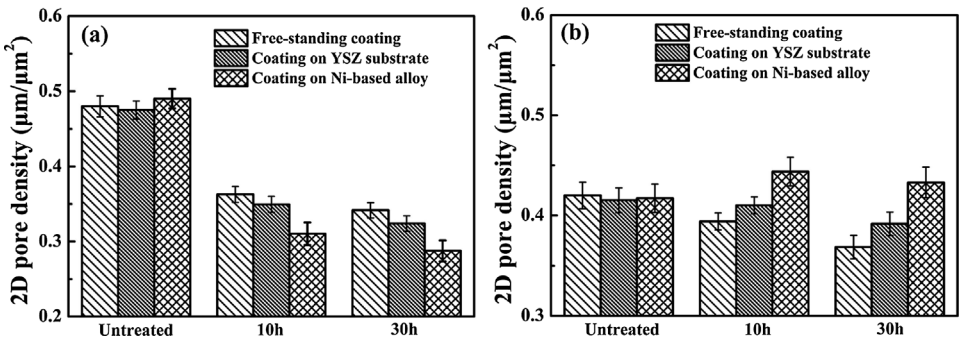

Fig. 5. Evolution of 2D pore densities as a function of thermal exposure duration: (a) inter-splat pores and (b) intra-splat cracks.

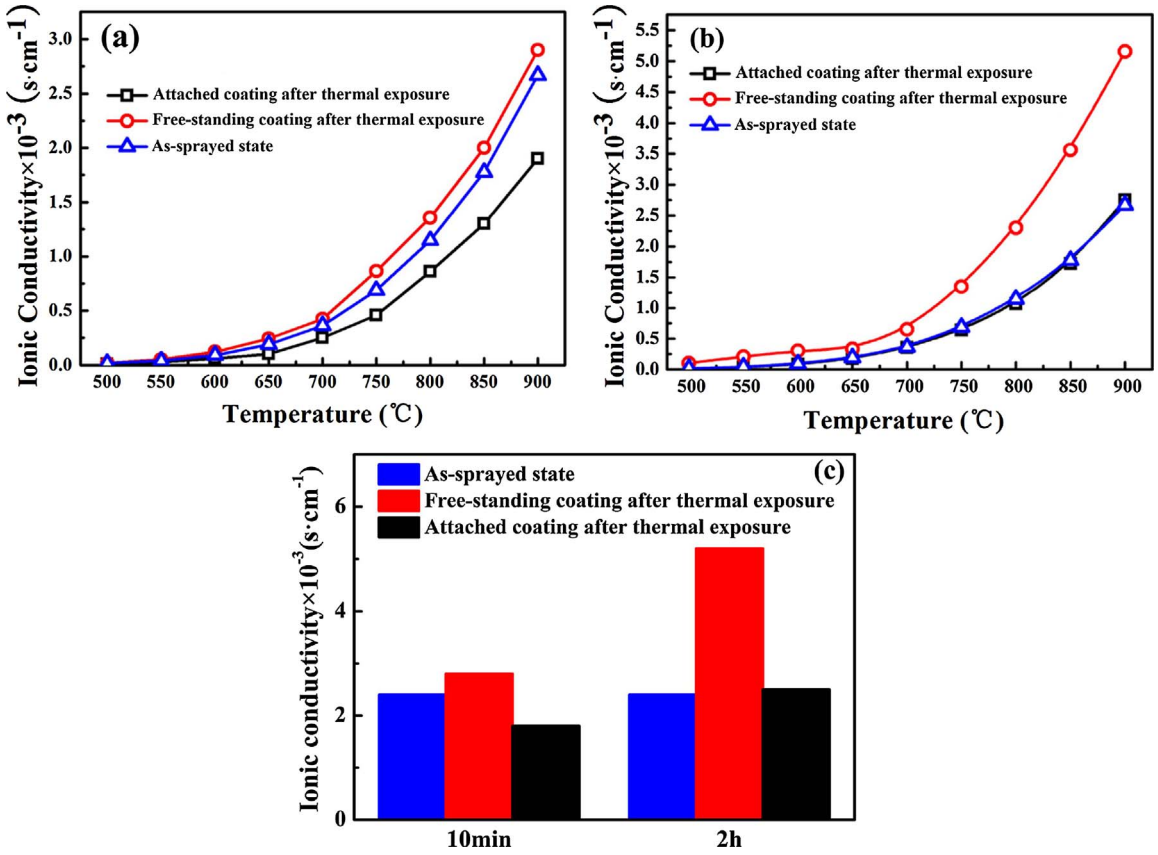

Fig. 6. Changes in ionic conductivity after thermal exposure for: (a) 10 min and (b) 2 h measured at different temperature. (c) is the comparison of ionic conductivity measured at 900 °C.

opportunities to connect in multi-points, and thus enhances their healing. On the contrary, the intra-splat cracks are widened under the CTE mismatch stress, as shown in a and a[1] in Fig. 10. Consequently, the healing of intra-splat cracks was retarded more or less.

3.4. Structural evolution after long thermal exposure

The constraint from CTE mismatch stress becomes more obvious with the increase of temperature and would hold for short time during

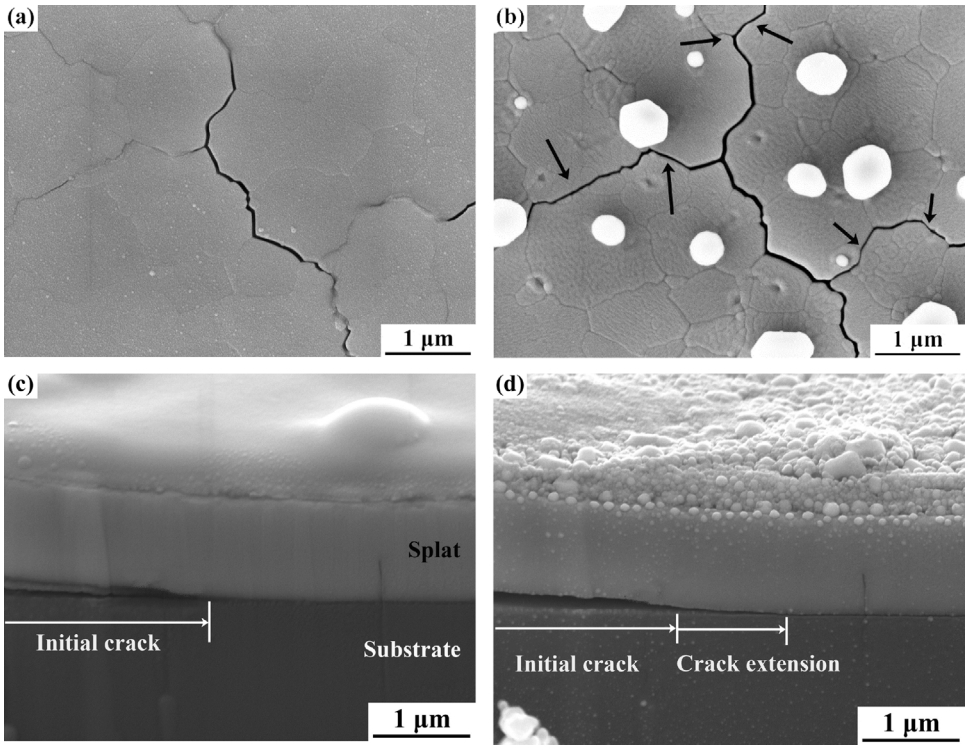

Fig. 7. Morphologies change after thermal exposure at 1100 °C for 10 min: (a) and (b) are intra-splat cracks before and after thermal exposure, respectively; (c) and (d) are inter-splat pores before and after thermal exposure, respectively.

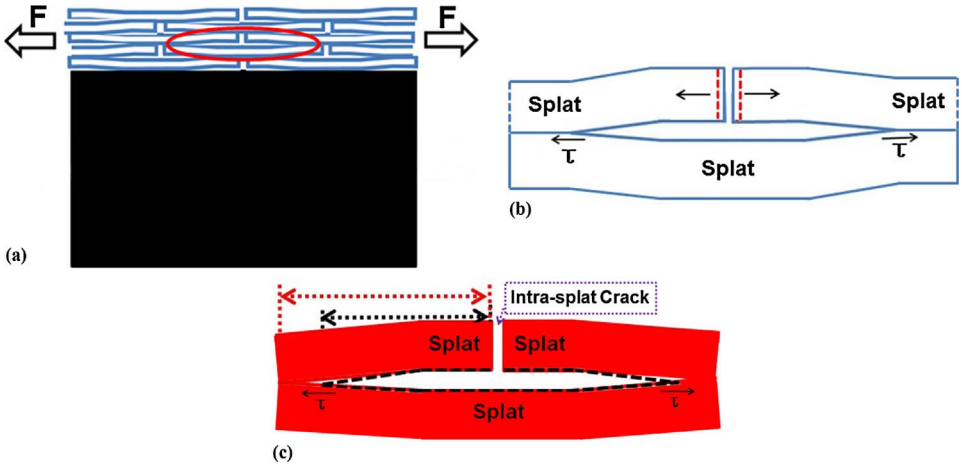

Fig. 8. Morphologies changes of 2D pores after thermal exposure: (a) a global view of coating attached to substrate, (b) force analysis of the 2D pores, and (c) morphologies changes in 2D pores.

thermal exposure. However, for long thermal exposure, creeping and cracking would relax some thermal stress and decrease the constraint on coating to some extent. Fig. 11 shows the morphology evolution of surface cracks in three different types of YSZ coatings after 100 h duration at 1100 °C. It can be found that the cracks in free-standing coating have been healed up, whereas the cracks in coating attached to YSZ substrate became narrowed a little. For coating attached to Ni-based superalloy, the cracks showed a little widening after 20 h duration. However, long time duration (100 h) also lead to obvious narrowing of cracks. Fig. 12 shows the global surface morphology of YSZ coatings after thermal exposure for 100 h. It can be found that some large scale cracks appeared on surface of the YSZ coating attached to Ni-based superalloy, since the coating became gradually stiffening owing to the healing of inter-splat pores [52]. The appearance of the large scale cracks resulted in stress relaxation. Consequently, the constraint effect was weakened. It is worth noting that the neighboring intra-splat cracks became narrowing, and thus enhanced the healing of these intra-splat cracks, as shown in Fig. 12. This is consistent with

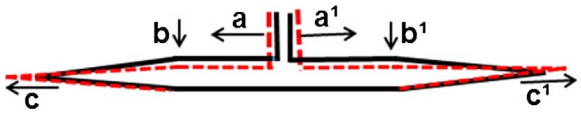

Fig. 10. Mechanisms of morphology changes in inter-splat pores and intra-splat cracks during thermal exposure.

previous report [19], which exhibit partial densification during constrained sintering. In brief, the substrate constraint results in anisotropic healing behavior of 2D cracks at heating stage and initial short duration. For a longer duration, the constrained effect would be weakened owing to globally cracking.

4. Conclusions

In this study, a detailed pore (or crack) healing behavior of plasma sprayed YSZ coatings was examined to understanding the constrained effect of substrate on the sintering of plasma sprayed ceramic coatings.

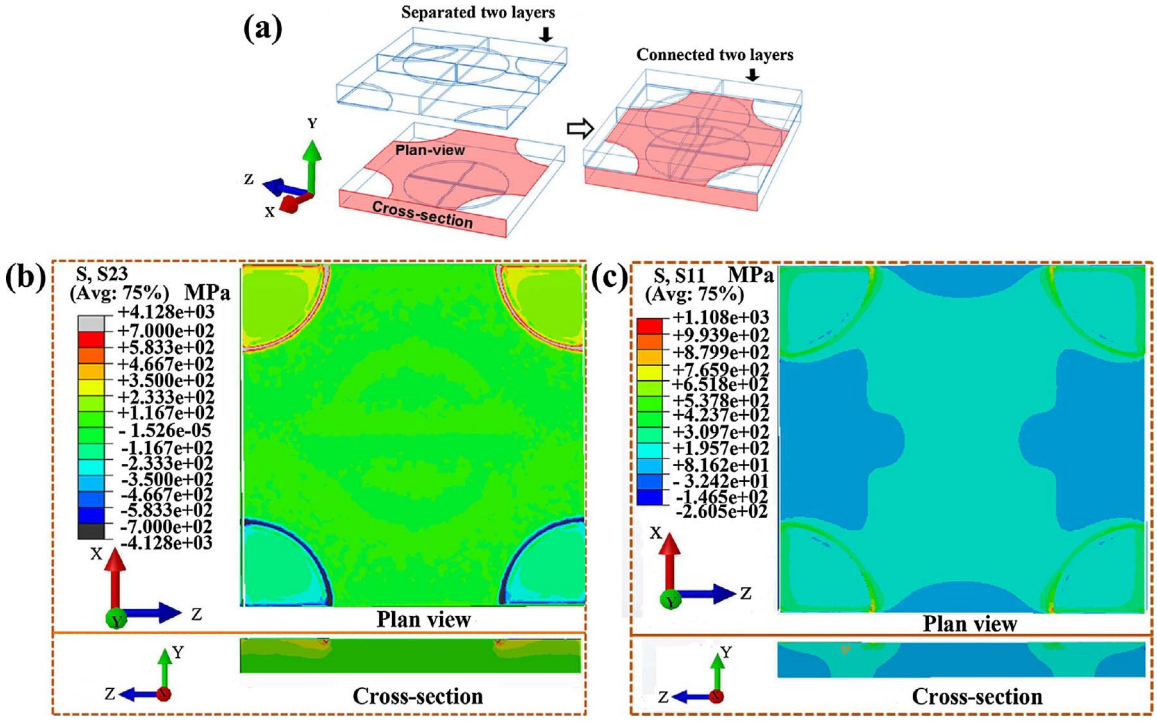

Fig. 9. Stress distribution in a splat under equally biaxial load along the x–z plane: (a) structural model of two layers; (b) shear stress concentrated at the bonding area (interface between two layers); (c) tensile stress inside a layer [40].

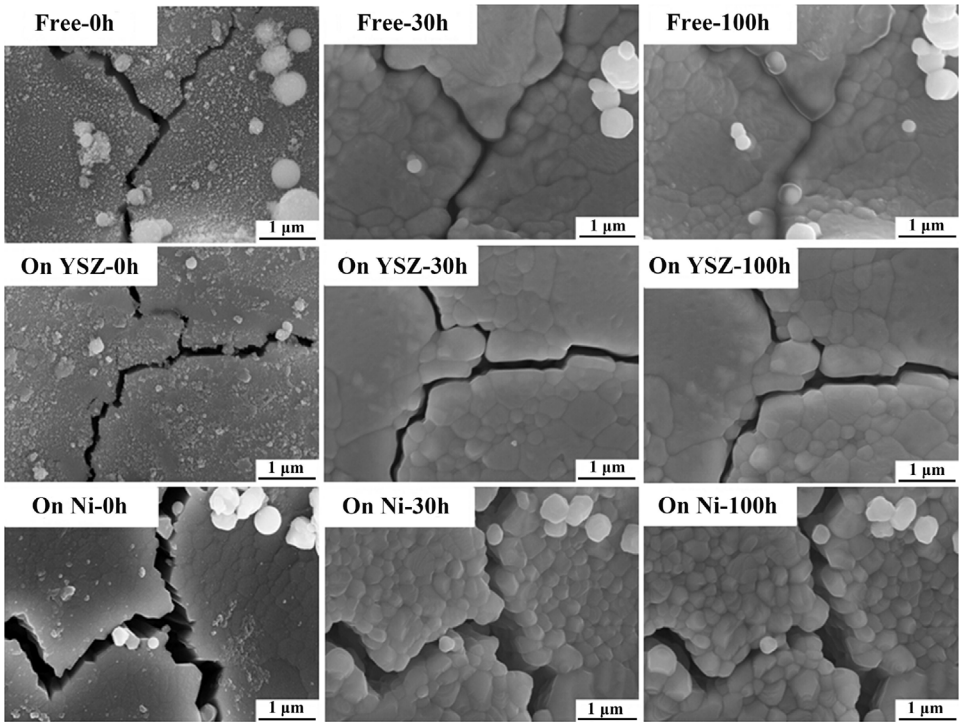

Fig. 11. Healing evolution of intra-splat cracks during long thermal exposure.

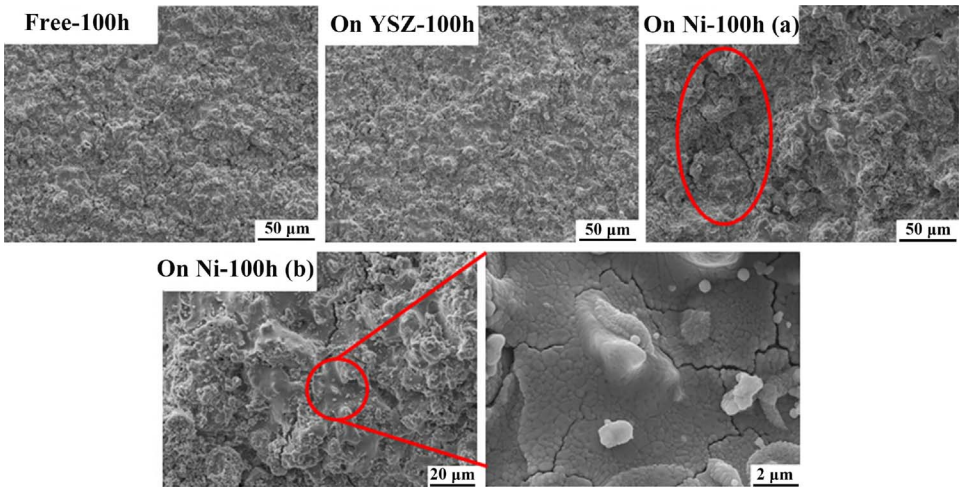

Fig. 12. Surface morphologies of different types of YSZ coatings after long thermal exposure.

Results showed that the structural changes during thermal exposure are stage-sensitive. In a relatively shorter thermal exposure, the inter-splat pores became narrowed, whereas the intra-splat cracks became widened. Consequently, these two kinds of microscale pores exhibit different healing kinetics. The healing kinetics of inter-splat pores was much faster than that of the intra-splat cracks. Correspondingly, the hardness in out-plane direction of the coating showed an enhanced increase with respect to that of the hardness in in-plane direction. In a relatively longer thermal exposure, some macroscale cracks appeared in coating surface owing to the gradually stiffening coatings. As a result, the microscale intra-splat cracks near the macroscale cracks were healed rapidly. In brief, the structural changes evolve from micro- to macro- scale as a function of the thermal exposure duration. This would benefit the further in-depth understanding of the thermal cycling failure mechanism of plasma sprayed TBCs.

Acknowledgments

The present project was supported by the National Basic Research Program of China (No. 2013CB035701), the Fundamental Research Funds for the Central Universities, and the National Program for Support of Top-notch Young Professionals.

References

[1] N.P. Padture, M. Gell, E.H. Jordan, Materials science - thermal barrier coatings for gas-turbine engine applications, Science 296 (5566) (2002) 280–284.
[2] R. Vassen, A. Stuke, D. Stover, Recent developments in the field of thermal barrier coatings, J. Therm. Spray Technol. 18 (2) (2009) 181–186.
[3] C.U. Hardwicke, Y.C. Lau, Advances in thermal spray coatings for gas turbines and energy generation: a review, J. Therm. Spray Technol. 22 (5) (2013) 564–576.
[4] Y.C. Zhou, H.M. Xiang, X.P. Lu, Z.H. Feng, Z.P. Li, Theoretical prediction on mechanical and thermal properties of a promising thermal barrier material: $Y4Al2O_9$, J. Adv. Ceram. 4 (2) (2015) 83–93.
[5] X.G. Chen, H.M. Zhang, H.S. Zhang, Y.D. Zhao, G. Li, $Ce_{1-x}Sm_xO_{2-x/2-A}$ novel type of ceramic material for thermal barrier coatings, J. Adv. Ceram. 5 (3) (2016) 244–252.
[6] J.A. Thompson, T.W. Clyne, The effect of heat treatment on the stiffness of zirconia top coats in plasma-sprayed TBCs, Acta Mater. 49 (9) (2001) 1565–1575.
[7] R.W. Trice, Y.J. Su, J.R. Mawdsley, K.T. Faber, A.R. De Arellano-Lopez, H. Wang, W.D. Porter, Effect of heat treatment on phase stability, microstructure, and thermal conductivity of plasma-sprayed YSZ, J. Mater. Sci. 37 (11) (2002) 2359–2365.
[8] S. Guo, Y. Kagawa, Young's moduli of zirconia top-coat and thermally grown oxide

in a plasma-sprayed thermal barrier coating system, Scripta Mater. 50 (11) (2004) 1401–1406.
[9] L. Xie, M.R. Dorfman, A. Cipitria, S. Paul, I.O. Golosnoy, T.W. Clyne, Properties and performance of high-purity thermal barrier coatings, J. Therm. Spray Technol. 16 (5–6) (2007) 804–808.
[10] S. Paul, A. Cipitria, S.A. Tsipas, T.W. Clyne, Sintering characteristics of plasma sprayed zirconia coatings containing different stabilisers, Surf. Coat. Tech. 203 (8) (2009) 1069–1074.
[11] R. Vassen, N. Czech, W. Mallener, W. Stamm, D. Stover, Influence of impurity content and porosity of plasma-sprayed yttria-stabilized zirconia layers on the sintering behaviour, Surf. Coat. Tech. 141 (2–3) (2001) 135–140.
[12] W.W. Zhang, G.R. Li, Q. Zhang, G.J. Yang, Comprehensive damage evaluation of localized spallation of thermal barrier coatings, J. Adv. Ceram. 6 (3) (2017) 230–239.
[13] T.W. Clyne, S.C. Gill, Residual stresses in thermal spray coatings and their effect on interfacial adhesion: a review of recent work, J. Therm. Spray Technol. 5 (4) (1996) 401–418.
[14] J. Matejicek, S. Sampath, Intrinsic residual stresses in single splats produced by thermal spray processes, Acta Mater. 49 (11) (2001) 1993–1999.
[15] X.J. Lu, P. Xiao, Constrained sintering of YSZ/Al_2O_3 composite coatings on metal substrates produced from eletrophoretic deposition, J. Eur. Ceram. Soc. 27 (7) (2007) 2613–2621.
[16] J. Matejicek, S. Sampath, In situ measurement of residual stresses and elastic moduli in thermal sprayed coatings - part 1: apparatus and analysis, Acta Mater. 51 (3) (2003) 863–872.
[17] X.C. Zhang, M. Watanabe, S. Kuroda, Effects of processing conditions on the mechanical properties and deformation behaviors of plasma-sprayed thermal barrier coatings: evaluation of residual stresses and mechanical properties of thermal barrier coatings on the basis of in situ curvature measurement under a wide range of spray parameters, Acta Mater. 61 (4) (2013) 1037–1047.
[18] M. Tillman, J.A. Yeomans, R.A. Dorey, The effect of a constraint on the sintering and stress development in alumina thick films, Ceram. Int. 40 (7) (2014) 9715–9721.
[19] X. Wang, A. Atkinson, Microstructure evolution in thin zirconia films: experimental observation and modelling, Acta Mater. 59 (6) (2011) 2514–2525.
[20] T.J. Garino, H.K. Bowen, Kinetics of constrained-film sintering, J. Am. Ceram. Soc. 73 (2) (1990) 251–257.
[21] J.S. Kim, R.A. Rudkin, X. Wang, A. Atkinson, Constrained sintering kinetics of 3YSZ films, J. Eur. Ceram. Soc. 31 (13) (2011) 2231–2239.
[22] C.J. Li, A. Ohmori, R. McPherson, The relationship between microstructure and Young's modulus of thermally sprayed ceramic coatings, J. Mater. Sci. 32 (4) (1997) 997–1004.
[23] H. Xie, Y.C. Xie, G.J. Yang, C.X. Li, C.J. Li, Modeling thermal conductivity of thermally sprayed coatings with intrasplat cracks, J. Therm. Spray Technol. 22 (8) (2013) 1328–1336.
[24] C.J. Li, A. Ohmori, Relationships between the microstructure and properties of thermally sprayed deposits, J. Therm. Spray Technol. 11 (3) (2002) 365–374.
[25] F. Cernuschi, P. Bison, S. Marinetti, E. Campagnoli, Thermal diffusivity measurement by thermographic technique for the non-destructive integrity assessment of TBCs coupons, Surf. Coat. Technol. 205 (2) (2010) 498–505.
[26] Y. Tan, A. Shyam, W.B. Choi, E. Lara-Curzio, S. Sampath, Anisotropic elastic properties of thermal spray coatings determined via resonant ultrasound spectroscopy, Acta Mater. 58 (16) (2010) 5305–5315.
[27] R.S. Lima, S.E. Kruger, G. Lamouche, B.R. Marple, Elastic modulus measurements via laser-ultrasonic and Knoop indentation techniques in thermally sprayed coatings, J. Therm. Spray Technol. 14 (1) (2005) 52–60.
[28] W.G. Chi, S. Sampath, H. Wang, Microstructure-thermal conductivity relationships for plasma-sprayed yttria-stabilized zirconia coatings, J. Am. Ceram. Soc. 91 (8) (2008) 2636–2645.
[29] T. Wakui, J. Malzbender, R.W. Steinbrech, Strain dependent stiffness of plasma sprayed thermal barrier coatings, Surf. Coat. Technol. 200 (16–17) (2006) 4995–5002.
[30] D.R. Clarke, C.G. Levi, Materials design for the next generation thermal barrier coatings, Annu. Rev. Mater. Res. 33 (2003) 383–417.
[31] D.R. Clarke, S.R. Phillpot, Thermal barrier coating materials, Mater. Today 8 (6) (2005) 22–29.
[32] D.R. Clarke, Materials selection guidelines for low thermal conductivity thermal barrier coatings, Surf. Coat. Technol. 163 (2003) 67–74.
[33] A. Ohmori, C.J. Li, Quantitative characterization of the structure of plasma-sprayed $Al2O_3$ coating by using copper electroplating, Thin Solid Films 201 (2) (1991) 241–252.
[34] A. Cipitria, I.O. Golosnoy, T.W. Clyne, A sintering model for plasma-sprayed zirconia TBCs. part I: free-standing coatings, Acta Mater. 57 (4) (2009) 980–992.
[35] A. Cipitria, I.O. Golosnoy, T.W. Clyne, A sintering model for plasma-sprayed zirconia thermal barrier coatings. part II: coatings bonded to a rigid substrate, Acta Mater. 57 (4) (2009) 993–1003.
[36] A.C.F. Cocks, N.A. Fleck, Constrained sintering of an air-plasma-sprayed thermal barrier coating, Acta Mater. 58 (12) (2010) 4233–4244.
[37] G.J. Yang, Z.L. Chen, C.X. Li, C.J. Li, Microstructural and mechanical property evolutions of plasma-sprayed YSZ coating during high-temperature exposure: comparison study between 8YSZ and 20YSZ, J. Therm. Spray Technol. 22 (8) (2013) 1294–1302.
[38] J. Ilavsky, J.K. Stalick, Phase composition and its changes during annealing of plasma-sprayed YSZ, Surf. Coat. Technol. 127 (2-3) (2000) 120–129.
[39] G.R. Li, H. Xie, G.J. Yang, G. Liu, C.X. Li, C.J. Li, A comprehensive sintering mechanism for TBCs-part I: an overall evolution with two-stage kinetics, J. Am. Ceram. Soc. 100 (5) (2017) 2176–2189.
[40] G.R. Li, G.J. Yang, C.X. Li, C.J. Li, Force transmission and its effect on structural changes in plasma-sprayed lamellar ceramic coatings, J. Eur. Ceram. Soc. 37 (8) (2017) 2877–2888.
[41] Y.Z. Xing, C.J. Li, Q. Zhang, C.X. Li, G.J. Yang, Influence of microstructure on the ionic conductivity of plasma-sprayed yttria-stabilized zirconia deposits, J. Am. Ceram. Soc. 91 (12) (2008) 3931–3936.
[42] M.J. Verkerk, B.J. Middelhuis, A.J. Burggraaf, Effect of grain-boundaries on the conductivity of high-purity ZrO2-$Y2O_3$ ceramics, Solid State Ionics 6 (2) (1982) 159–170.
[43] D. Perez-Coll, E. Sanchez-Lopez, G.C. Mather, Influence of porosity on the bulk and grain-boundary electrical properties of Gd-doped ceria, Solid State Ionics 181 (21–22) (2010) 1033–1042.
[44] Y.Z. Xing, C.J. Li, C.X. Li, G.J. Yang, Influence of through-lamella grain growth on ionic conductivity of plasma-sprayed yttria-stabilized zirconia as an electrolyte in solid oxide fuel cells, J. Power Sources 176 (1) (2008) 31–38.
[45] G.R. Li, B.W. Lv, G.J. Yang, W.X. Zhang, C.X. Li, C.J. Li, Relationship between lamellar structure and elastic modulus of thermally sprayed thermal barrier coatings with intra-splat cracks, J. Therm. Spray Technol. 24 (8) (2015) 1355–1367.
[46] F. Kroupa, J. Dubsky, Pressure dependence of Young's moduli of thermal sprayed materials, Scripta Mater. 40 (11) (1999) 1249–1254.
[47] C. Zhang, C.J. Li, G. Zhang, X.J. Ning, C.X. Li, H.L. Liao, C. Coddet, Ionic conductivity and its temperature dependence of atmospheric plasma-sprayed yttria stabilized zirconia electrolyte, Mat. Sci. Eng. B-Solid 137 (1–3) (2007) 24–30.
[48] F. Ahmed, K. Bayerlein, S.M. Rosiwal, M. Goken, K. Durst, Stress evolution and cracking of crystalline diamond thin films on ductile titanium substrate: analysis by micro-raman spectroscopy and analytical modelling, Acta Mater. 59 (14) (2011) 5422–5433.
[49] U.A. Handge, Analysis of a shear-lag model with nonlinear elastic stress transfer for sequential cracking of polymer coatings, J. Mater. Sci. 37 (22) (2002) 4775–4782.
[50] Y. Leterrier, Durability of nanosized oxygen-barrier coatings on polymers - internal stresses, Prog. Mater. Sci. 48 (1) (2003) 1–55.
[51] G.R. Li, G.J. Yang, C.X. Li, C.J. Li, Strain-induced multiscale structural changes in lamellar thermal barrier coatings, Ceram. Int. 43 (2) (2017) 2252–2266.
[52] G.R. Li, B. Cheng, G.J. Yang, C.X. Li, Strain-induced stiffness-dependent structural changes and the associated failure mechanism in TBCs, J. Eur. Ceram. Soc. 37 (11) (2017) 3609–3621.